INTERNATIONAL JOURNAL OF AUTOMOTIVE AND MECHANICAL ENGINEERING
ISSN: 2229-8649 e-ISSN: 2180-1606
VOLUME 23, ISSUE 3, 2026, 13925 - 13940
DOI: https://doi.org/10.15282/ijame.23.3.2026.14.1050

RESEARCH ARTICLE

Multi-objective optimization of parallel hydraulic flushing circuit based on NSGA-II

Yan Cao, Bing Zhang, Jingding Tian, Jiawei Wu, Hongyu Lu, Hao Chen*

School of Mechanical Engineering, Jiangsu University, 212013 Zhenjiang, Jiangsu, China

Abstract - In the parallel flushing circuit for large-scale hydraulic motor testing, increasing the flushing flow rate increases the total pressure loss and casing pressure differential, whereas reducing the pipeline pressure loss alone increases the casing pressure. To solve this strongly conflicting engineering problem, this study proposes an optimization method that combines the Maximin Latin Hypercube Sampling, Kriging surrogate model, and NSGA-II algorithm. Specifically, five core design variables (pipeline length, elbow quantity, and pump flow) were systematically tuned to minimize the casing pressure difference, total pressure loss, and flushing flow. The TOPSIS method was further applied to derive optimal solutions under different design preferences. The method was verified via AMESim simulation and leave-one-out cross-validation, achieving 0.8%–10.1% optimization for each target, and provides a valuable engineering reference for multi-objective optimization of similar hydraulic circuits. In conclusion, the proposed multi-objective optimization framework successfully resolved the inherent physical contradiction between casing heat dissipation and mechanical seal safety. This proves that the combination of the MLHS, Kriging surrogate models, and NSGA-II is a highly robust approach for large-scale hydraulic test bench design.

Article History
Received : 10 April 2026
Revised : 28 April 2026
Accepted : 11 June 2026
Published : 30 September 2026

Keywords
Large-scale hydraulic motor
Parallel flushing circuit
Motor test bench
Hydraulic circuit optimization
Multi-objective optimization
AMESim

1. Introduction

Large-scale hydraulic motors, characterized by high torque, low speed, and precise transmission control, are increasingly being used in engineering applications such as loaders, mining equipment, and marine vessels [1]-[2]. Consequently, the testing of large-scale hydraulic motors after production and assembly plays a crucial role in ensuring their reliability during long-term high-intensity operations under harsh working conditions. Taking the testing of Hägglunds large-scale internal curve radial piston hydraulic motors as an example, this study focuses on the flushing circuit that removes a large amount of heat and metal debris generated inside the motor casing during testing. The overall optimization of this circuit is of great significance for the testing of large-scale hydraulic motors, which can last several weeks. Owing to the long test cycle and high test power of large-scale hydraulic motors, the adoption of traditional testing methods inevitably consumes a large amount of electrical energy during the test, leading to a sharp increase in test costs. In response to this characteristic, a dual-motor torque-opposing mode was adopted in the testing process: the torque generated by the tested hydraulic motor during the test was transmitted to the main shaft of another hydraulic motor of the same model through the central shaft, which was called the loading motor. This method not only creates and simulates the load in actual use for the tested motor, but also allows the loading motor to be used as a hydraulic pump to convert the torque generated by the tested motor back into electrical energy and feed it into the test power grid [3]. This dual-hydraulic-motor torque-opposing testing method significantly reduces the energy consumption cost during the entire test period and is suitable for large-scale hydraulic motor testing. A 3D schematic of the test bench is shown in Figure 1.

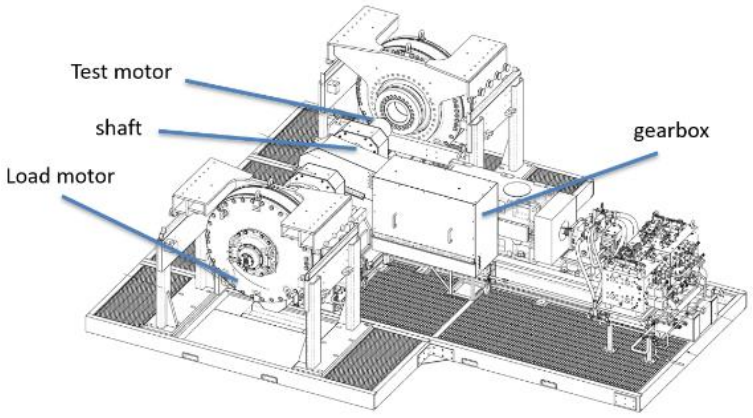


Figure 1. 3D Schematic diagram of the hydraulic motor test bench

Although the dual-motor torque-opposing testing method is beneficial for reducing the test costs, accompanying problems have also emerged. Although the loading motor operates as a hydraulic pump during the test, it requires a separate flushing circuit to cool and flush its casing. Owing to the large number and high complexity of the entire test bench system, a simple arrangement of the flushing circuit is prone to excessive pressure loss and unbalanced pressure

***CORRESPONDING AUTHOR | Hao Chen|** ✉ mahaochen@gmail.com
© 2026 The Authors. Published by Universiti Malaysia Pahang Al-Sultan Abdullah Press. This is an open access article under the CC BY-NC 4.0 license

between the two motor casings. Moreover, unlike the piston chamber of a motor, the internal casing of a piston motor cannot withstand excessive pressure. As a sealing component, the maximum pressure that the shaft seal can withstand is relatively low (the pressure resistance of the shaft seal for this test model should not exceed 3 bar). Second, poor flushing conditions [4] and relatively high pressure [5] adversely affect the service life of the sealing components. In addition, owing to the design factors of the test bench, the relative pressure difference between the two motor casings is more likely to cause accelerated wear and premature failure of the sealing components under long-term testing conditions [6]. Because the loading motor is part of the test bench, the above-mentioned problems are more likely to occur when replacing different tested motors and conducting long-term tests under different working conditions. In summary, optimizing the hydraulic flushing circuit for a large-scale hydraulic motor test bench is important.

In recent years, many scholars have conducted extensive research on the optimization of hydraulic circuits and reduction of pressure loss. Among the various components, elbows have become a key research focus because of their significant local resistance. In Reference [7], the author reduced the local resistance of elbows by innovatively designing the structure of elbows in hydraulic systems and conducting a simulation analysis using simulation software. Recent research [8] proposed the integration of novel double-sharp guide vanes within hydraulic elbows to simultaneously address additive manufacturing constraints and optimize internal flow fields. This structural innovation effectively disrupts large-scale vortices, achieving a 47.29% reduction in the peak pressure drop and significantly lowering the turbulent kinetic energy. To address the design complexities of additively manufactured hydraulic valves, scholars have developed a parametric mathematical model to rapidly predict the pressure loss in curved internal channels [9]. By combining CFD simulations and experimental validation, this method accurately characterizes the flow resistance with an error of 7.72%, significantly enhancing the design efficiency of hydraulic systems. Reference [10] conducted multiple test experiments on pipelines with different parameters and performed quantitative research on the pressure loss at pipeline elbows. Reference [11] considered the turbulent flow state and all important conditions in the study of liquid flow in elbows and optimized various parameters using genetic algorithms. The critical nature of pressure loss in hydraulic systems continues to drive innovative research. For instance, recent studies have investigated the microscopic fluid dynamics and fundamental mechanisms of hydraulic pressure loss under complex vertical transport conditions [12], further emphasizing the necessity of accurately mapping the wall shear stress and local resistance in fluid networks. To quantify and mitigate energy inefficiencies in mobile hydraulic drives, recent studies have utilized MATLAB SIMULINK to simulate pressure drops across complex pipeline networks [13]. Their analysis revealed that accurately optimizing the internal diameter of critical line segments can reduce the frictional power loss by over 80%, providing a highly effective strategy for energy recovery and system efficiency improvement. To simplify the structure of multi-motor hydraulic systems, recent studies have proposed a novel six-position, six-way direction control valve and systematically evaluated its flow-pressure loss characteristics [14]. The experimental results indicated that the maximum pressure loss is highly dependent on the valve's specific operating position and internal flow direction, highlighting the necessity of precisely evaluating the localized resistance in complex hydraulic configurations.

For the hydraulic flushing circuit, the timely removal of the heat generated by the hydraulic motor during testing is one of its main functions. To mitigate thermal accumulation in the continuous fluid recirculation of hydrostatic transmissions, recent studies [15] have optimized the design and control of hydraulic flushing circuits. By implementing an intelligent temperature-dependent control strategy for the flushing valve, the system dynamically regulates the flushing flow, effectively preventing overheating and significantly reducing overall energy losses. In the realm of advanced thermal management, recent research [16] has explored the efficacy of specialized microchannel heat sinks that utilize vertical fluid flushing and jet impingement. By systematically evaluating local heat transfer characteristics, studies have confirmed that targeted fluid flushing strategies can significantly enhance cooling efficiency and maintain surface temperatures within strict safety margins under high heat fluxes. Similarly, Reference [17] indicated that when a non-traditional oil cooling system is used, the volume flow rate of the cooling oil significantly affects heat dissipation. Although these studies establish the importance of the cooling flow, they often treat it as an independent control variable. A major conflicting operational trade-off in practical applications is that indiscriminately increasing the flushing flow to enhance heat dissipation exponentially exacerbates the pipeline pressure loss, which is a severe physical contradiction that prior single-objective optimization studies have largely overlooked.

When optimizing hydraulic circuits, simulation software can greatly facilitate the analysis of fluid flow in pipelines and subsequent optimization. To accurately evaluate the pressure drop and thermal-hydraulic characteristics within complex flow channels, recent studies [18] have extensively used advanced numerical simulation software. By incorporating real fluid property modules and robust turbulence models, computational simulations provide a highly reliable framework for analyzing localized flow resistance and heat transfer under diverse boundaries and operating conditions. AMESim software has proven to be an indispensable tool for analyzing energy consumption and mitigating throttling losses in modern pump-controlled hydraulic circuits [19]. Utilizing this dynamic simulation environment, scholars have successfully modelled complex pressure behaviors under variable working conditions, providing a robust virtual testing ground that bridges the gap between theoretical algorithm design and physical experimental validation. To address the severe energy dissipation inherent in traditional hydraulic circuits, scholars [20] have proposed novel flow-sharing architectures aimed at minimizing wasted energy. Utilizing lumped parameter simulation environments such as AMESim, these studies successfully quantified the energy-saving potential and pressure loss reduction achieved by the optimized valve designs, further validating their industrial-scale applicability. Additionally, Reference [21] combined AMESim with genetic algorithms to design a hydraulic control system, optimize the system's power loss through the algorithm, and improve the system's performance. The introduction of the optimization algorithm has been of great help

in solving these problems. To tackle complex combinatorial optimization challenges in manufacturing scheduling, recent research [22] introduced the Teaching Learning-Based Optimization (TLBO) algorithm. Extensive computational experiments demonstrated that TLBO significantly outperforms traditional metaheuristic algorithms, such as particle swarm optimization and grey wolf optimization, exhibiting superior search efficiency and the highest average performance ranking in minimizing comprehensive production costs. By leveraging an optimized algorithmic approach to conduct multi-time scale dispatch, researchers [23] achieved substantial reductions in total scheduling costs and a remarkable 13.98% improvement in system response speed, highlighting the robust capability of intelligent algorithms in enhancing system flexibility and economic benefits of the system. To enhance the control accuracy and performance of electromechanical servo systems, a novel dual-motor synchronized control algorithm was proposed [24]. This algorithmic optimization significantly improved the dynamic response and load control precision of the system, demonstrating its effectiveness in advanced motor servo applications. Despite these advancements in algorithm application, a significant scalability issue arises when 3D computational fluid dynamics (CFD) or 1D simulation software is directly coupled with heuristic algorithms. For large-scale hydraulic systems, this direct-coupling approach incurs prohibitive computational costs and time during the massive iterative evaluation process, making it difficult to scale up to complex multi-objective scenarios. Among them, the NSGA-II multi-objective optimization algorithm [25] is one of the optimal methods for solving related hydraulic circuit optimization problems, as it can address the issue of "synergistic optimization of multiple conflicting objectives," enable multi-angle objective optimization under multi-parameter conditions, and cover a wide range of parameter optimization combinations. Beyond hydraulic systems, the NSGA-II algorithm has demonstrated a robust capability to resolve complex fluid-mechanical conflicts in other automotive applications. For instance, researchers [26] successfully applied NSGA-II to optimize vehicle exhaust mufflers, achieving an optimal Pareto balance between maximizing the acoustic transmission loss and minimizing the fluid pressure drop. Reference [27] suggests that the NSGA-II multi-objective optimization algorithm was combined with a neural network to establish an optimization model; with pressure loss set as one of the optimization objectives, the pressure loss was reduced by 9.0% after optimization. Furthermore, Reference [28] proposed a new hybrid algorithm based on the NSGA-II multi-objective optimization algorithm to achieve better optimization of the target hydraulic system and verified the effectiveness of this method in reducing the pressure loss of the target system.

Researchers have conducted detailed studies on hydraulic circuit optimization from various perspectives, covering both theoretical and experimental testing. Recently, surrogate-assisted multi-objective optimization has become a prominent trend in fluid power systems owing to its computational efficiency. This optimization trend is rapidly evolving in the literature. Recent advanced frameworks have successfully integrated computational fluid dynamics (CFD) with the NSGA-II algorithm to optimize the hydraulic performance of complex multiphase pumps [29] and applied genetic algorithms to balance hydraulic efficiency with broader economic and sustainability metrics [30]. Furthermore, to ensure computational efficiency without sacrificing solution fidelity, highly precise Kriging surrogate models combined with novel intelligent algorithms have been increasingly adopted to reduce performance fluctuations in multi-objective engineering tasks [31]**.** Several recent studies (2022-2024) have successfully applied Kriging, RBF, or ANN combined with NSGA-II to optimize individual hydraulic components, such as multi-way valves and single piping networks. Specifically, existing surrogate model applications conventionally assume deterministic, fixed boundary conditions (e.g., a constant inlet flow rate). Therefore, they are fundamentally ill-equipped to adequately address the strongly coupled pressure loss versus flow rate conflict inherent in parallel circuits. In a parallel layout, modifying the geometric resistance of one branch does not merely alter its own localized pressure drop; instead, it dynamically redistributes the flow across all constituent branches. This nonlinear kinetic redistribution constantly shifts the operating points of the entire system, rendering conventional static surrogate mapping ineffective and necessitating a fully coupled multi-objective framework. However, a critical gap remains in existing surrogate-based frameworks, which primarily focus on isolated, single-branch systems, where objective conflicts are relatively straightforward. However, they fall short in addressing the highly coupled and asymmetric fluid dynamics inherent in large-scale parallel hydraulic test benches. In such parallel circuits, altering the geometry of one branch nonlinearly redistributes the flow and amplifies the pressure differential across the entire system, creating a much stronger and more complex multi-objective conflict. To justify the methodological shift from traditional single-objective approaches to a multi-objective framework, the physical outcomes of these algorithms must be contrasted. In highly coupled hydraulic circuits, single-objective pipeline optimization inevitably drives the system toward unacceptable operational extremes, such as minimizing pressure loss by drastically reducing the flushing flow, which consequently causes thermal failure of the motor. In contrast, a multi-objective framework mathematically internalizes these physical contradictions. It captures the exact trade-off boundaries (Pareto front) between the cooling capacity and seal safety, ensuring that the optimization of one parameter does not cause the catastrophic degradation of another. Therefore, adopting a multi-objective methodology is not merely an algorithmic preference but an engineering necessity for parallel flushing circuits. To bridge this gap, this study does not merely apply existing algorithms but customizes a holistic surrogate-assisted framework specifically for severe multi-objective conflicts in large-scale parallel flushing circuits. The original contributions of this study are threefold: we establish a highly accurate Kriging-based predictive model trained via MLHS, successfully decoupling the complex nonlinear flow-pressure interactions in a parallel hydraulic layout; the study quantitatively reveals the underlying physical trade-off mechanisms between flushing cooling capacity and the mechanical safety boundaries of motor shaft seals, yielding a comprehensive Pareto optimal front; by integrating the TOPSIS method, the framework provides a scalable parameter-selection strategy, allowing engineers to dynamically adapt the circuit design according to varying power loads and test duration requirements of different hydraulic motors. In this study, the AMESim simulation software and NSGA-II multi-objective optimization

algorithm were used to analyze and optimize a parallel hydraulic flushing circuit. The optimization aims to reduce the casing pressure of the two motors, reduce the casing pressure difference, and decrease the pressure loss of the two parallel flushing circuits, realizing multi-factor and multi-objective optimization to lower these values to a smaller range. In this framework, a mathematical model was formulated to systematically balance hydraulic conflicts. Therefore, the overarching objective of this study is to develop a robust surrogate-assisted multi-objective optimization framework capable of decoupling highly nonlinear flow–pressure interactions in large-scale parallel hydraulic test benches. By systematically mapping the physical trade-off boundaries, this study aims to provide a reliable theoretical basis and a flexible engineering decision-making tool to fundamentally resolve the industrial conflict between heat dissipation demands and mechanical seal safety. The specific research objectives of this study are explicitly defined as follows: (1) minimizing the casing pressure difference $\left(\left|P_{\mathrm{A}}-P_{\mathrm{B}}\right|\right)$ to ensure the mechanical safety of the motor seals; (2) minimizing the total pressure loss $\left(PL_{\mathrm{A}}+PL_{\mathrm{B}}\right)$ to reduce the system energy consumption; and (3) maximizing the pump flow (Q) to guarantee sufficient cooling and flushing capacity during continuous testing. While increasing the safety margin, the optimized circuit is also suitable for the subsequent testing of motors with larger displacements, thereby meeting the actual engineering requirements. The proposed multi-objective framework effectively reconciles the industrial conflict between heat dissipation and mechanical safety, offering a robust and scalable decision-making roadmap for the design and maintenance of large-scale hydraulic test benches.

2. Materials and Methods

2.1 Basic Data

The motor test used a pair of large inner-curve radial piston hydraulic motors of the Hägglunds CB400400 model. The hydraulic circuit for flushing the casings adopts an Eaton vane pump with a maximum flow rate of 96 L/min. The flushing oil is No. 46 anti-wear hydraulic oil, and its viscosity index can ensure that the viscosity of the motor remains stable under the working conditions of 5–60 °C, avoiding the increase in casing pressure difference caused by viscosity fluctuation. The circuit was mainly constructed using seamless steel pipes with an inner diameter of 22 mm and a wall thickness of 3 mm, and 90-degree elbows with an inner diameter of 22 mm and a 1.5D (dimension). Five pressure sensors of the Danfoss MBS3250 model were installed at the outlet of the oil pump, the inlets of the two branches, and the casings of the tested motor and loading motor, and their pressure measurement range was 0–600 bar. The connection between the flushing circuit and motor casing was established using a hose with an inner diameter of 32 mm. A schematic of the structure of the flushing circuit is shown in Figure 2(a).

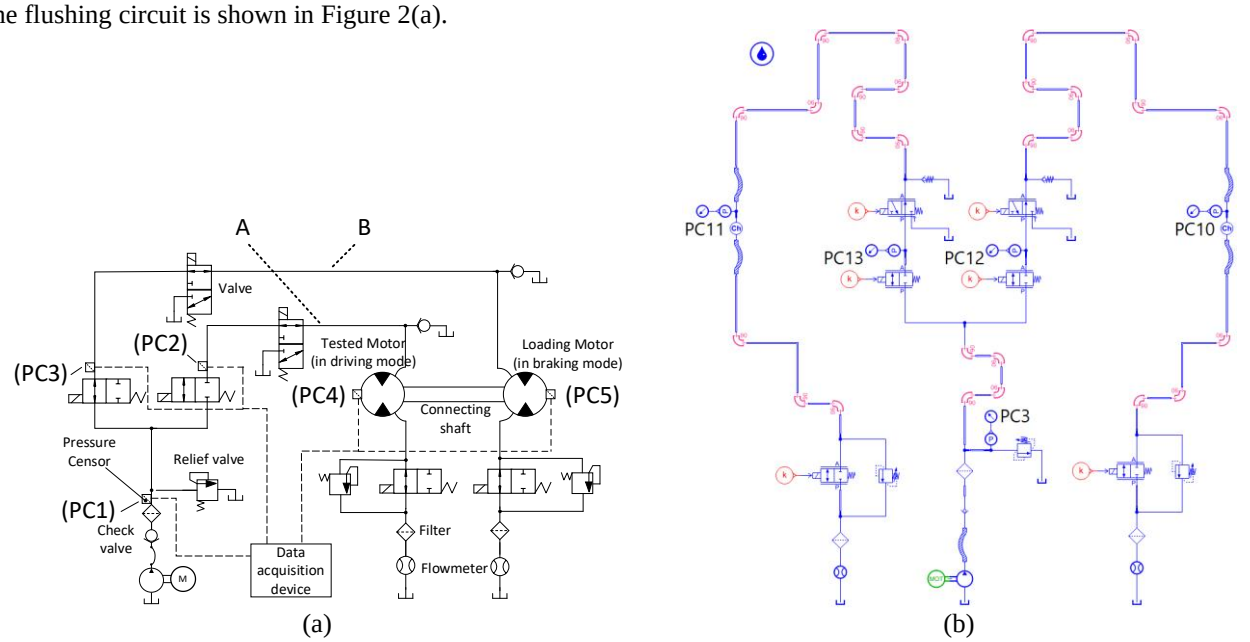


Figure 1. Overview of the parallel hydraulic flushing system and simulation model validation. (a) 3D Schematic diagram of hydraulic motor test bench; (b) Schematic diagram of hydraulic flushing circuit structure; (c) Simulation model of the flushing circuit

2.2 Mathematical Modelling of Pressure Loss and Heat Dissipation

Because the flow of hydraulic oil in pipelines inevitably causes pressure loss, the value of this pressure loss can be determined using formulas. Among them, the pressure loss of hydraulic oil flowing through a straight pipeline can be calculated using the Darcy-Weisbach Eq. (1):

$$\Delta p_{\mathrm{f}}=\lambda\frac{l}{d}\frac{\rho v^{2}}{2} \tag{1}$$

The local pressure loss occurring at the elbows of the circuit can be calculated using Eq. (2):

$$\Delta p_{\mathrm{r}} = \varsigma \frac{\rho \upsilon^2}{2} \tag{2}$$

The total pressure loss was calculated using Eq. (3):

$$\Delta p = \sum \lambda_{\mathrm{i}} \frac{l_{\mathrm{i}}}{d_{\mathrm{i}}} \frac{\rho \upsilon_{\mathrm{i}}^2}{2} + \sum \varsigma_{\mathrm{i}} \frac{\rho \upsilon_{\mathrm{i}}^2}{2} \tag{3}$$

In the formula, l represents the pipeline length; d denotes the pipeline inner diameter; λ stands for the frictional resistance coefficient; ς is the local resistance coefficient; υ indicates the average flow velocity of the liquid inside the pipeline; ρ represents the fluid density.

Because removing the heat generated by the motor during testing is one of the main purposes of the flushing circuit, the heat in the motor casing originates from the total power loss of the motor, which is expressed by the following formulas:

$$P_{\mathrm{m}} = C \cdot P_{\mathrm{o}} \tag{4}$$

$$P_{\mathrm{t}} = P_{\mathrm{m}} + P_{\mathrm{v}} \tag{5}$$

In Eqs. (4) and (5), C denotes the mechanical loss coefficient, P_{o} is the motor output power, P_{m} and represents the mechanical loss power. P_{t} represents the total loss power, and P_{v} is the volume loss power.

For the tested motor, the case flushing flow rate was calculated using Eq. (6):

$$q_{\mathrm{f}} = 3.4\left(P_{\mathrm{t}} - P_{\mathrm{a}}\right) \tag{6}$$

In Eq. (6) q_{f} represents the flushing flow rate of one motor case and P_{a} denotes the natural heat dissipation power of the motor case to air.

From these basic equations, it can be concluded that the main causes of pressure loss in the hydraulic circuit are the length of the pipelines and the number of bends. Moreover, the flow rate required by the motor during testing was determined using the flow rate calculation formula. Therefore, the target parameters for optimizing the hydraulic system can be obtained.

2.3 Model Establishment and Experimental Validation

2.3.1 Collection of test parameters

The pressure difference between the inlet and outlet of the tested motor was set to 150 bar, and the rotational speed was set to 25 rpm. After the loading test was run for a period of time, the flushing oil pump started automatically, and the flushing flow rate was adjusted according to the temperature sensor at the motor casing. Once the experiment stabilized for 30 s, pressure data from the pressure sensors at various positions were collected. A set of data was collected every 2 s, and the process was repeated thrice. The average of these three sets of data was calculated to form one group of experimental data. This procedure of waiting for stabilization and averaging multiple independent trials was strictly implemented to filter out random fluctuations and ensure the repeatability of the experiment. Furthermore, owing to the industrial scale of the test bench, the overall measurement uncertainty is predominantly determined by the inherent accuracy of the calibrated instruments (Type B uncertainty). The technical specifications and maximum uncertainties of the key measurement instruments used in the circuit are listed in Table 1. Given that the relative errors between the AMESim simulation and experimental results (Section 2.3.3) were largely within the combined uncertainty bounds of these industrial sensors, the robustness of the simulation model was considered validated for subsequent surrogate modelling. Six groups of experimental data were collected, as shown in Table 2.

Table 1. Technical specifications and measurement uncertainty of key instruments

Instrument Type	Model	Measurement Range	Accuracy / Maximum Uncertainty
Pressure Sensor	Danfoss MBS3250	0 – 600 bar	±0.5% Full Scale (FS)
Flowmeter	Industrial Gear Flowmeter	0 – 96 L/min	±0.5% of reading

Table 2. Experimental data of the flushing circuit

Number	PC1/bar	PC2/bar	PC3/bar	PC4/bar	PC5/bar	Pumping Flow (L/min)
1	3.62	2.18	2.04	0.82	0.73	62.78
2	3.71	2.24	2.05	0.79	0.74	62.14
3	3.66	2.20	2.03	0.80	0.73	61.60
4	4.49	2.66	2.44	0.96	0.84	69.77
5	4.51	2.68	2.49	0.95	0.85	69.94
6	4.31	2.56	2.44	0.92	0.84	67.70

2.3.2 Establishing AMEsim model

After the measurement and data collection, the main parameters of the test bench and hydraulic oil used are presented in Table 3. AMESim software was used to model and simulate the hydraulic flushing circuit. First, a physical model was constructed sequentially using four modules: Sketch, Submodel, Parameter, and Simulation. The specific steps are as follows.

i) In the Sketch mode, components such as the pump, hydraulic motor, filter, directional control valve, and 90° elbows were connected in sequence according to the schematic diagram of the flushing circuit of the test bench.
ii) In the Submodel mode, an appropriate submodel was selected for each component. Then, in the parameter mode, parameters including the pump flow rate, pipeline inner diameter and length, and elbow curvature radius were defined.
iii) In the Simulation mode, click "Run" to operate the simulation model.

Because the interior of the motor casing requiring flushing is a closed chamber, the "Simple hydraulic chamber" component was selected as a substitute. In addition, considering the flushing circuit characteristics of medium-length pipelines and no significant oil fluctuation, the HL0001/2/3 and HRBP0011E Submodels, which only account for capacitance and resistance, were chosen for all pipelines and elbows. For the other hydraulic components, submodels were selected, and their parameter information was filled in with reference to the technical manuals provided by the manufacturers. The established model is illustrated in Figure 2(b).

Table 3. Parameters of the test bench

Parameter	Values
A Pipeline length/m	9.3
B Pipeline length/m	10.5
A Number of elbows	8
B Number of elbows	8
Hydraulic oil density / (kg· m^{-3})	0.88×103
Absolute viscosity /（Pa· s）	0.042
bulk modulus/MPa	1.5×103
motor case capacity/cm^3	0.7×106

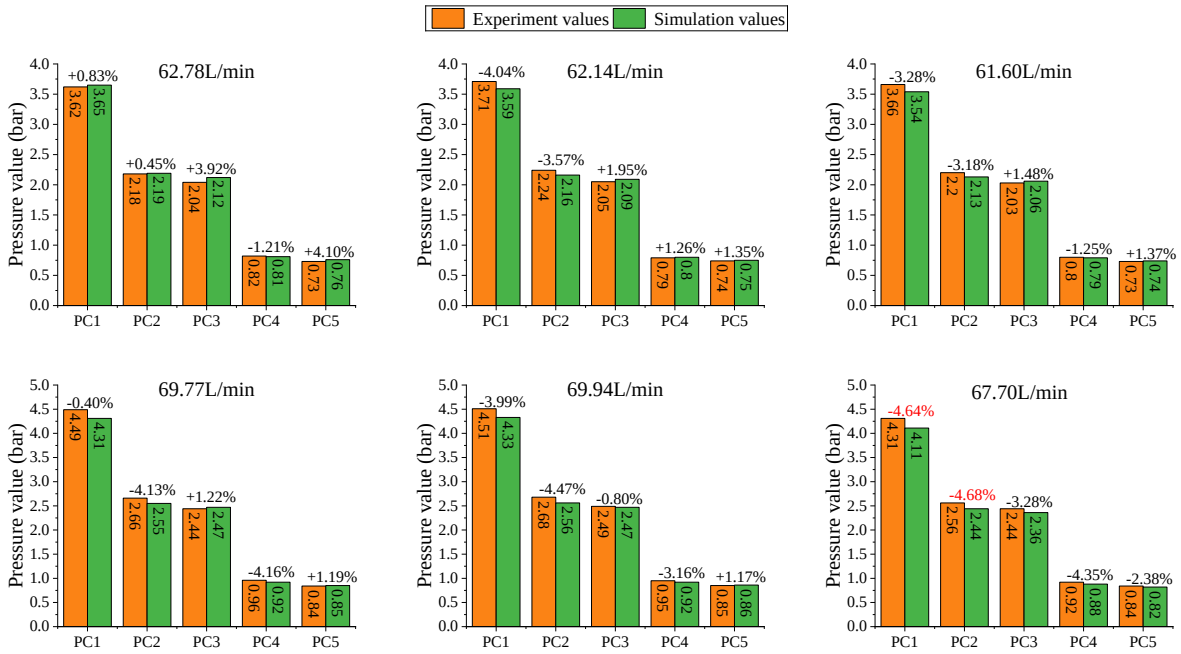


Figure 3. Comparison between simulation and test data

2.3.3 Verification and accuracy analysis of the simulation model

Simulation data were obtained by simulating the six groups of working conditions derived from the tests, and a comparison was made between these simulation data and the motor test data, as shown in Figure 3. The simulation error values were calculated using the following Eq. (7).

$$\mathrm{RE} = \frac{|V_e - V_s|}{V_e} \cdot 100\% \tag{7}$$

where RE represents the Relative Error, V_e denotes the Experimental Value and V_s is Simulation Value.

From the red-marked parameters of the simulation group with a flow rate of 67.70 L/min in Figure 3, it can be observed that two sets of data have relatively large relative errors (errors greater than 4.5%). This is mainly caused by the error in the sensor data collection in the experimental tests and the inability of the simulation software to fully simulate the complex working conditions of the hydraulic flushing circuit during actual operation. However, the errors between all simulation data and experimental values were within 5%, which is within the acceptable range in engineering practice; therefore, this simulation model can be used for the next optimization work.

2.4 Range of Parameter Values

Given the large number of subsystems within the motor test bench, the hydraulic flushing circuit, which is one of these subsystems, must be routed around other systems during the pipeline layout. Excessively long pipelines increase the frictional pressure loss, whereas excessively short pipelines require more elbows for connection, thereby increasing the local pressure loss. Therefore, based on the actual conditions of the test bench, the value ranges for the Pipeline A length and number of elbows were determined for the two parallel flushing circuits: the pipeline for the tested motor (hereafter referred to as Pipeline A) and the pipeline for the loading motor (hereafter referred to as Pipeline B). In addition, the value range for the flushing circuit pump flow rate was calculated using the above equations. These are presented in Table 4, which defines the value boundaries for the subsequent hydraulic system optimization.

Table 4. Range of parameters

Parameter	Minimum Values	Maximum Values
Pipeline A length/m	6.5	9.5
Pipeline B length/m	9	12
A Number of elbows	4	8
B Number of elbows	6	9
Pump flow / (L/min)	60	70

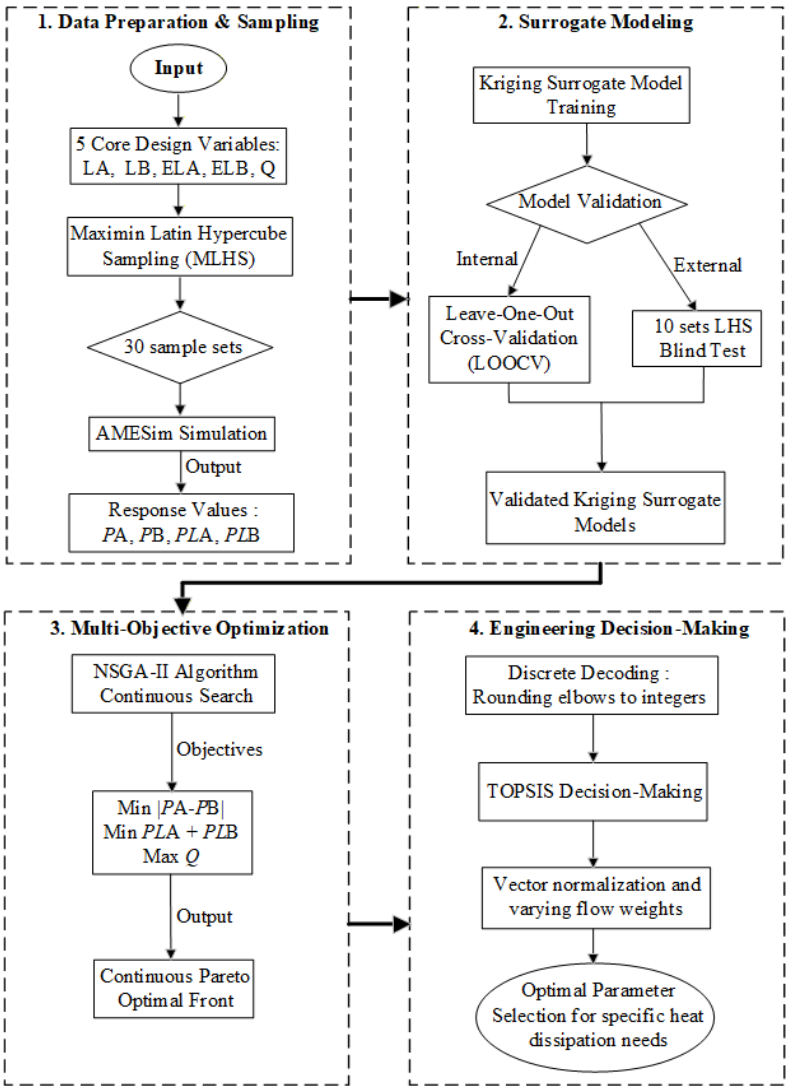


Figure 4. Unified flowchart of the proposed multi-objective optimization framework

3. Results and Discussion

3.1 Experimental Design

After determining the optimal design variables, a multi-objective optimization model for the flushing circuit was established, and its mathematical model is given by Eq. (8):

$$\text{Minimise: } \{ f_1(x), f_2(x), f_3(x), f_4(x), f_5(x) \} \tag{8}$$

In the mathematical model:

$$f_1(x) = f_{P1}(x) \tag{9}$$

$$f_2(x) = f_{P2}(x) \tag{10}$$

$$f_3(x) = | f_{P1}(x) - f_{P2}(x) | \tag{11}$$

$$f_4(x) = f_{PL1}(x) + f_{PL2}(x) \tag{12}$$

$$f_5(x) = -Q \tag{13}$$

$$x = [L_A, L_B, EL_A, EL_B, Q]^T \tag{14}$$

where, L_A, L_B, EL_A, EL_B, Q respectively represents the length of Pipeline A, the length of Pipeline B, the number of elbows in Pipeline A, the number of elbows in Pipeline B, and the pump flow rate; $f_1(x), f_2(x), f_3(x), f_4(x), f_5(x)$ denotes the optimization objectives, among them: $f_3(x)$ stands for the pressure difference between the casings of motor A and motor B; $f_4(x)$ is the sum of pressure losses in Pipeline A and Pipeline B; $f_5(x)$ represents the objective of maximizing flow, and it takes a negative value. $f_{P1}(x), f_{P2}(x), f_{PL1}(x), f_{PL2}(x)$ respectively represent the surrogate models: motor casing pressure value at side A, motor casing pressure value at side B, pressure loss of pipeline A, and pressure loss of pipeline B. Figure 4 shows the flowchart of the complete research method.

Table 5. Sampling values and corresponding response values

	Sampling Values					Response Values			
	LA/m	LB/m	ELA	ELB	Q(L/min)	P1/bar	P2/bar	PL1/bar	PL2/bar
1	8.475	10.510	5	7	64.301	0.8402	0.7636	1.2181	1.3047
2	8.561	9.849	8	7	67.802	0.8973	0.8133	1.3451	1.4092
3	9.272	10.189	5	7	68.174	0.8902	0.8181	1.3629	1.4357
4	8.734	11.895	7	8	60.589	0.7998	0.7121	1.1254	1.2279
5	7.768	10.467	7	7	65.660	0.8713	0.7802	1.2488	1.3465
6	8.025	10.908	8	8	66.211	0.8799	0.7870	1.2836	1.3863
7	7.689	10.005	7	9	62.127	0.8197	0.7342	1.1310	1.2208
8	7.122	11.916	6	7	69.890	0.9407	0.8294	1.3777	1.5362
9	7.441	10.884	6	8	61.898	0.8200	0.7279	1.1182	1.2320
10	6.616	9.558	7	8	60.083	0.7918	0.7061	1.0333	1.1306
11	8.357	9.175	5	9	63.080	0.8294	0.7504	1.1674	1.2310
12	7.038	11.579	4	7	65.760	0.8802	0.7748	1.2251	1.3747
13	7.845	11.632	8	8	61.300	0.8117	0.7199	1.1239	1.2384
14	9.302	10.651	6	6	62.495	0.8210	0.7427	1.1881	1.3516
15	6.524	9.068	5	9	64.481	0.8554	0.7636	1.1559	1.2603
16	6.746	9.790	5	6	68.418	0.9132	0.8152	1.2931	1.4067
17	7.283	11.146	7	8	66.366	0.8859	0.7856	1.2631	1.3920
18	9.110	11.465	5	9	60.877	0.8026	0.7171	1.1358	1.2298
19	8.979	10.361	7	7	61.524	0.8159	0.7356	1.1631	1.2920
20	6.835	10.269	5	7	63.422	0.8421	0.7478	1.1387	1.2555
21	9.406	9.961	7	7	67.446	0.8901	0.8104	1.3562	1.4059
22	8.678	9.344	4	8	65.147	0.8588	0.7780	1.2402	1.3027
23	7.977	9.299	6	8	62.883	0.8273	0.7471	1.1537	1.2225
24	9.015	11.715	6	6	64.935	0.8607	0.7707	1.2675	1.3640
25	8.817	11.208	5	9	67.272	0.8955	0.8008	1.3350	1.4405
26	7.565	9.445	8	8	63.973	0.8441	0.7605	1.1850	1.2618
27	8.273	9.673	7	6	68.973	0.9148	0.8285	1.3693	1.4372
28	8.187	10.701	6	8	69.385	0.9260	0.8293	1.3867	1.4921
29	7.301	11.062	4	7	69.205	0.9280	0.8226	1.3443	1.4830
30	6.916	11.331	5	6	66.98	0.8967	0.792	1.2626	1.4059

3.2 Maximin Latin Hypercube Sampling

The research object of this study was a 5-dimensional mixed-variable model. To achieve uniform coverage of all operating conditions in the parameter space while minimizing the workload of simulation sampling, Maximin Latin Hypercube Sampling (MLHS) was adopted to obtain experimental samples. Latin Hypercube Sampling (LHS) is a computer-aided experimental design method based on stratified sampling [32], whose core principle is to evenly divide the value range of each design variable into n non-overlapping subintervals (where n denotes the sample size), randomly select one sample point within each subinterval, and then randomly pair the sampling values of each variable to form n groups of parameter combinations, ensuring that the full value range of each variable is covered. To address the problem that the basic LHS is prone to sample aggregation and difficult to cover blind areas in high-dimensional space, this study introduces the Maximin criterion to optimize the sampling results: through iterative adjustment of sample pairing combinations, the minimum Euclidean distance between all sample points is maximized, so that the sample points are uniformly distributed in the 5-dimensional space, avoiding sample aggregation and achieving blind-area-free coverage of operating conditions for multi-variable combinations. Because the number of design variables in this study is five, according to the relevant criteria in the field of engineering optimization, the sampling size n must be greater than or equal to five times the number of design variables, and n=30 is considered here. After 30 groups of sampling samples were obtained by the above method in MATLAB, they were substituted into the validated AMESim simulation model for numerical analysis of each combination, and the response values of the corresponding optimization objectives were obtained, as shown in Table 5.

3.3 Establishment of The Kriging Model

To support the massive iterative calculations required for subsequent multi-objective optimization, a Kriging surrogate model was adopted to construct a nonlinear mapping relationship between the design variables and optimization objectives. The Kriging model is a surrogate model based on the best linear unbiased estimation, which is specifically designed for computer experiments. Its response relationship is formed by the superposition of a global trend term and a stationary Gaussian stochastic process term, enabling the high-precision fitting of black-box systems while outputting uncertainty quantification metrics for the prediction results. In this study, independent Kriging surrogate models were constructed for the motor casing pressure values at sides A and B, motor casing pressure differential, and total circuit pressure loss: the 5-dimensional design variables were input through MATLAB software, with 30 groups of MLHS samples and their corresponding AMESim response values used as the training dataset. The Gaussian squared exponential kernel, which is universally applied in the engineering field, was selected as the kernel function, and the optimal hyperparameters of the model were solved using the maximum likelihood estimation method to complete the model training.

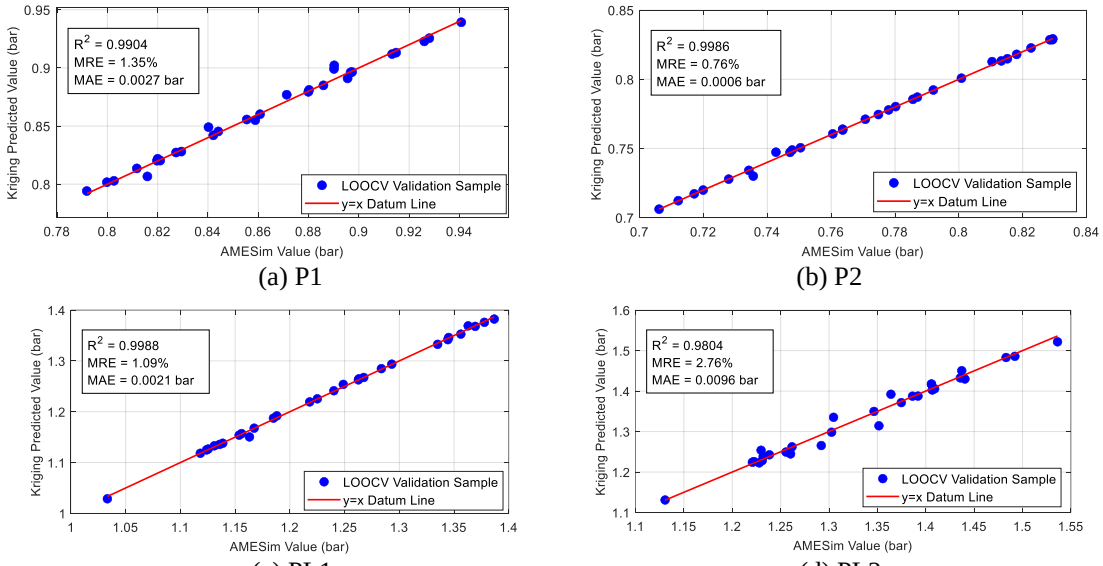


Figure 4. Cross-validation results plots

To verify the accuracy and validity of the established surrogate models, the leave-one-out cross-validation (LOOCV) method was adopted in this study. The operating principle of LOOCV is as follows: one group is reserved from the 30 samples as the test set each time, and the remaining 29 groups are used as the training set; a Kriging model is trained with the 29 groups each time to predict the response value of the reserved 1 group of samples; after 30 cycles, cross-validation prediction values for all 30 groups of samples are obtained. These cross-validation prediction values were compared with the real values from the AMESim simulation, and the coefficient of determination R^2, Maximum Relative Error (MRE), and Mean Absolute Error (MAE) were calculated to assess the internal fitting accuracy of the models. However, while LOOCV provides a reliable measure of internal consistency, relying solely on these internal metrics is insufficient to fully establish the external generalization capability of the models in a highly nonlinear space. Therefore, an additional rigorous validation utilizing completely unseen test data was introduced, as detailed in Section 3.3.1. The parity plots obtained

from the validation are shown in Figure 5. Among them, the coefficients of determination R^2 of the surrogate models for motor casing pressure differential and total circuit pressure loss are 0.9904, 0.9986, 0.9988, and 0.9804, respectively; the maximum relative errors are 1.35%, 0.76%, 1.09%, and 2.67%, respectively; the Mean Absolute Errors (MAE) are 0.0027 bar, 0.0006 bar, 0.0021 bar, and 0.0096 bar, respectively. All LOOCV validation samples in the plots are closely and uniformly distributed on both sides of the y=x reference line without systematic deviation, which verifies the prediction stability of the models in the full design space.

3.3.1 Justification of sample adequacy and external validation

While the internal LOOCV metrics demonstrate high fitting accuracy, relying solely on 30 MLHS samples for a 5-dimensional space raises theoretical concerns regarding potential overfitting and uncaptured nonlinear interactions. An external blind test was conducted to rigorously justify the adequacy of the sample size and evaluate the true generalization capability of the Kriging models. An independent test set comprising 10 unseen sample configurations was generated using the Standard Latin Hypercube Sampling (LHS) method. These configurations were simulated in AMESim to obtain the ground truth, which was then compared with the predictions of the established Kriging models. The validation results revealed that the Maximum Relative Error (MRE) for the motor casing pressures was constrained below 1.2%, and the MRE for the total pressure losses was strictly below 5.2%. Such consistently low prediction errors for completely unseen randomized LHS configurations explicitly demonstrate that the models accurately captured the underlying physical fluid dynamics without overfitting. Consequently, it was confirmed that the 30 MLHS samples comprehensively covered the feasible design space, proving that the sample size was computationally efficient and fundamentally adequate for this specific parallel circuit optimization.

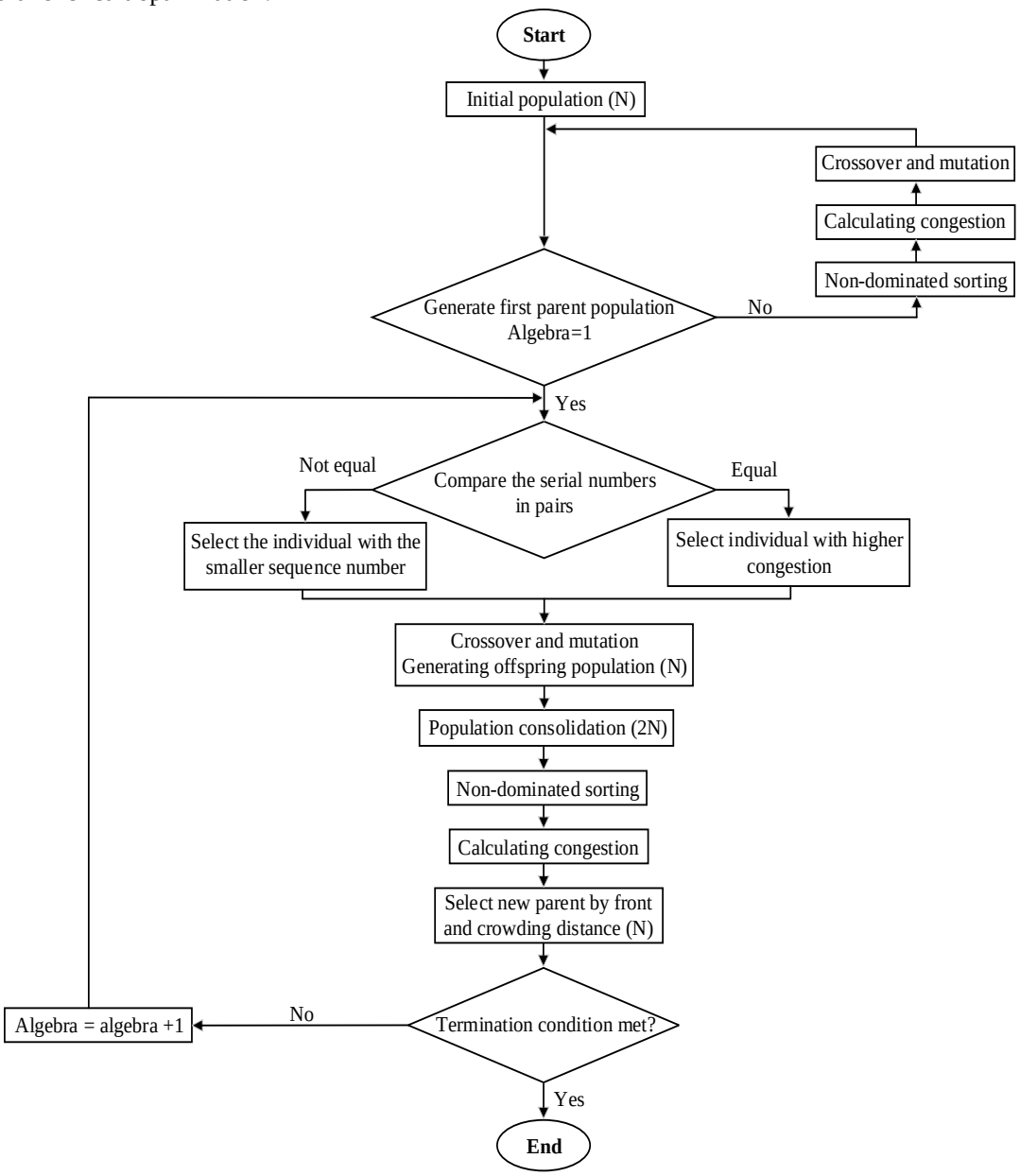


Figure 6. The process of multi-objective optimization algorithm

3.4 Multi-Objective Optimization Algorithm

The core of the multi-objective algorithm, Non-dominated Sorting Genetic Algorithm II (NSGA-II), lies in simulating the biological evolution process to search for the Pareto optimal solution set among "multiple conflicting optimization objectives." The Pareto optimal solution set refers to a collection of solutions in which improving one objective inevitably impairs at least one other objective. Specifically, NSGA-II evolves a randomly generated initial population into a larger offspring population through dominance sorting, selection, crossover, and mutation. Subsequently, fast non-dominated sorting is performed to create a new parent population. Finally, the offspring population generated by the genetic algorithms was combined with the parent population to form a new population. This algorithm continuously repeats the above steps until the set conditions are met, as shown in Figure 6. It can be concluded from the mathematical formulas listed earlier that although an increase in the flow rate can optimize the heat dissipation efficiency of the motor casing, it will also lead to an increase in pressure loss. Moreover, because Pipelines A and B are in a parallel relationship, changing the parameters of one pipeline will affect the other. Therefore, the research object in this study meets the condition of searching for the optimal solution among "multiple conflicting optimization objectives."

To balance the continuous search mechanism of the NSGA-II algorithm with the discrete nature of industrial piping components, a 'continuous search, discrete decoding' strategy was implemented in this study. During the algorithmic iteration phase, the integer constraints on the number of elbows (*EL*A and *EL*B) were deliberately relaxed, treating them as continuous variables. This relaxation is crucial because enforcing strict integer constraints during the evolutionary process of the genetic algorithm would cause the Pareto front to collapse into disconnected discrete layers, severely impairing the ability of the algorithm to maintain population diversity and fully explore the highly nonlinear fluid dynamics space. Subsequently, during the final engineering decision-making phase, a 'rounding to the nearest integer' mathematical constraint was applied to these variables before the TOPSIS evaluation. This ensures that the final parameters rigorously conform to the available standardized industrial components.

To balance the continuous search mechanism of the NSGA-II algorithm with the discrete nature of industrial piping components, a 'continuous search, discrete decoding' strategy was implemented in this study. During the algorithmic iteration phase, the integer constraints on the number of elbows (*EL*A, *EL*B) were deliberately relaxed, treating them as continuous variables. This relaxation is crucial; enforcing strict integer constraints during the genetic algorithm's evolutionary process would cause the Pareto front to collapse into disconnected discrete layers, severely impairing the algorithm's ability to maintain population diversity and fully explore the highly non-linear fluid dynamics space. Subsequently, during the final engineering decision-making phase, a 'rounding to the nearest integer' mathematical constraint was applied to these variables before the TOPSIS evaluation. This ensures that the finalized parameters rigorously conform to available standardized industrial components.

3.5 Optimization Results

After the Kriging models were successfully validated, the NSGA-II algorithm was executed using MATLAB software. Instead of arbitrary selection, the algorithm hyperparameters were configured based on established literature benchmarks in surrogate-assisted hydraulic optimization [27]-[28] to ensure a strict balance between the convergence speed and population diversity. Specifically, the parameters for obtaining the optimal solution set were determined as follows: population size = 200, maximum number of iterations = 400, crossover probability = 0.8, mutation probability = 0.2, and elite retention ratio = 0.1. The optimization weights of the five optimization objectives in formula (8) were set to 0.200, 0.200, 0.200, 0.200, and 0.200, respectively. The corresponding three-dimensional plot of the Pareto front is shown in Figure 7. The plot shows that the Pareto solution set covers the feasible region of the objective space, and the two-dimensional projection plot of the Pareto optimal solution set shown in Figure 8 clearly reflects the trade-off relationship among the three conflicting objectives: the pressure differential and total pressure loss increase synchronously with the increase in pump flow rate, which is consistent with the actual engineering law.

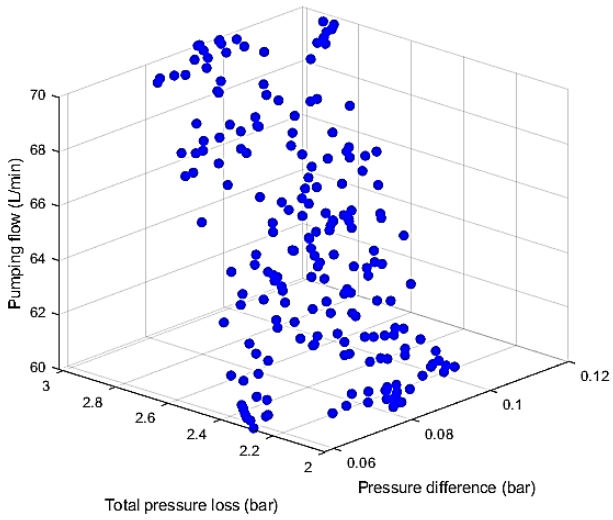


Figure 7. Three-dimensional plot of the pareto frontta

To objectively evaluate and select the final engineering parameters from the Pareto optimal set, the Technique for Order Preference by Similarity to Ideal Solution (TOPSIS) was employed. First, to eliminate dimensional discrepancies among the three physical objectives (pressure difference, pressure loss, and flow rate), the objective matrix was standardized using vector normalization. Subsequently, the normalized matrix was multiplied by the specific weight vectors. The weight assignment rationale was strictly driven by practical testing constraints: to maintain baseline system safety, the relative weights for the pressure difference and pressure loss were kept equal; meanwhile, the weight for the pump flow was dynamically adjusted (as listed in Table 6) to accommodate the varying heat dissipation demands of different tested motors. Finally, the Euclidean distance metric was used to calculate the distance of each candidate solution from the positive ideal solution (D^+) and the negative ideal solution (D^-). The solutions were ultimately ranked based on their relative closeness coefficient, calculated as $C = \frac{D^-}{D^+ + D^-}$, allowing engineers to identify the optimal parameter combinations for specific thermal load conditions. It should be noted that while the TOPSIS evaluation yields mathematically exact values for pipeline lengths (e.g., 9.49 m), real-world implementation is inherently subject to engineering constraints. Standardized manufacturing dimensions for seamless steel pipes, the discrete availability of industrial elbows, and inevitable on-site installation tolerances dictate that these algorithmic outputs serve as guiding baselines, rather than rigid specifications. In practice, engineers must map these theoretical optima to the nearest commercially available standard component. This physical deviation further underscores the necessity of obtaining a uniformly distributed Pareto front, as it provides a robust spectrum of alternative near-optimal solutions when the adoption of exact parameters is practically constrained.

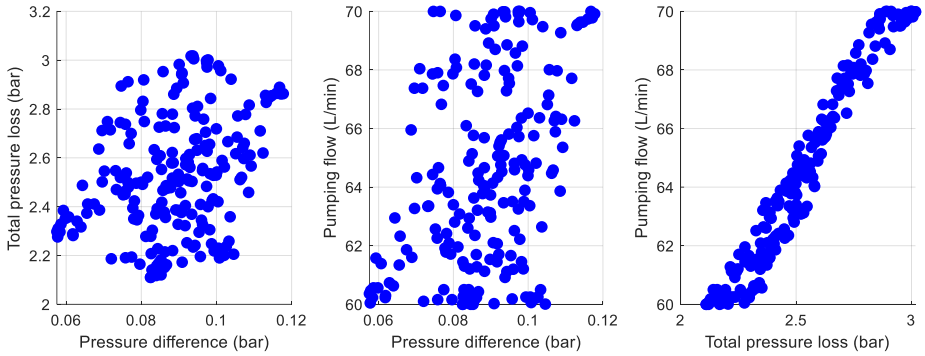


Figure 8. Two-dimensional projection plot of the pareto optimal solution

Additionally, in Table 5, three sets of parameter combinations are identical. This phenomenon arises because the Pareto optimal solution set converges to the same parameter combination within this flow rate interval, which belongs to the optimization plateau period in the iterative-solution process. By setting different weights for the flow rate, the algorithm can derive the optimal solution for the parameter combination under the corresponding working conditions. In practical engineering, for low-load test scenarios or the testing of low-power hydraulic motors, a parameter combination with a smaller flow weight can be selected to achieve energy consumption savings. For high-load test scenarios or the testing of higher-power hydraulic motors, a parameter combination with a larger flow weight can be selected to better remove the impurities and heat generated in the motor casing during the test.

Table 6. Optimal solution sets under different flow weights

Parameters Values						Objective Values			
Flow weights	LA /m	LB /m	ELA	ELB	Q (L/min)	Case A pressure /bar	Case B pressure /bar	Pressure differential /bar	Total pressure loss/bar
0.200	9.50	9.04	5	7	60.05	0.7779	0.7201	0.0578	2.2760
0.225	9.49	9.04	5	7	60.36	0.7823	0.7248	0.0575	2.2977
0.250	9.38	9.05	5	7	61.58	0.7997	0.7404	0.0593	2.3844
0.275	9.38	9.05	5	7	61.58	0.7997	0.7404	0.0593	2.3844
0.300	9.49	9.04	5	7	67.38	0.8812	0.8116	0.0696	2.7117
0.325	9.38	9.04	5	7	68.04	0.8911	0.8201	0.0710	2.7483
0.350	9.38	9.04	5	7	68.04	0.8911	0.8201	0.0710	2.7483
0.375	9.48	9.00	5	8	70.00	0.9206	0.8459	0.0747	2.8941
0.400	9.48	9.00	5	8	70.00	0.9206	0.8459	0.0747	2.8941

The Pareto optimal solutions presented above reveal a strict physical trade-off inherent to parallel hydraulic circuits. From a fluid dynamics perspective, increasing the pumping flow enhances the heat dissipation and debris-flushing capacity within the motor casings. However, higher flow velocities exponentially increase the fluid friction against the pipe walls (on-way resistance) and exacerbate localized flow separation at the elbows (local resistance), causing an

inevitable surge in the total pressure loss. Furthermore, owing to the asymmetric geometric layout of the two parallel branches (variances in pipe lengths and elbow quantities), increasing the total flow disproportionately amplifies the dynamic pressure drops between Pipelines A and B. This fluid kinetic divergence directly induces a casing pressure difference. Therefore, the Pareto front represents the physical and engineering contradictions between maximizing the cooling capability of the system and protecting the vulnerable motor shaft seals from excessive asymmetric pressure loads

The Pareto optimal solutions presented above reveal a strict physical trade-off inherent to the parallel hydraulic circuit. From a fluid dynamics perspective, increasing the pumping flow enhances the heat dissipation and debris flushing capacity within the motor casings. However, higher flow velocities exponentially increase fluid friction against the pipe walls (on-way resistance) and exacerbate localized flow separation at the elbows (local resistance), causing the inevitable surge in total pressure loss. Furthermore, due to the asymmetric geometric layout of the two parallel branches (variances in pipe lengths and elbow quantities), increasing the total flow disproportionately amplifies the dynamic pressure drops between Pipeline A and B. This fluid kinetic divergence directly induces the casing pressure difference. Therefore, the Pareto front essentially represents the physical and engineering contradiction between maximizing the system's cooling capability and protecting the vulnerable motor shaft seals from excessive asymmetric pressure loads.

3.5.1 Comparative analysis of optimization algorithms

To rigorously justify the selection of the NSGA-II algorithm over other heuristic methods, a comparative analysis was conducted using a Multi-objective Pattern Search (MOPS) algorithm as an alternative benchmark. Both optimization processes were driven by the same validated Kriging surrogate models under comparable evaluation budgets. As shown in Figure 9, a clear distinction in solution diversity was observed. The alternative MOPS algorithm (marked by red crosses) successfully approached the optimal trade-off surface but suffered from significant local clustering, failed to explore the full extent of the optimal front, and left obvious coverage gaps. Conversely, the NSGA-II algorithm (marked by blue solid circles) demonstrated a superior population diversity, yielding a uniformly distributed and expansive Pareto optimal set. This robust and continuous spread of non-dominated solutions is a direct consequence of the crowding distance operator of NSGA-II, which effectively prevents premature convergence to a narrow region. For the parallel hydraulic flushing circuit, obtaining such a diverse and uniform Pareto front is essential, as it provides a comprehensive and unbiased spectrum of design alternatives for the subsequent TOPSIS evaluation.

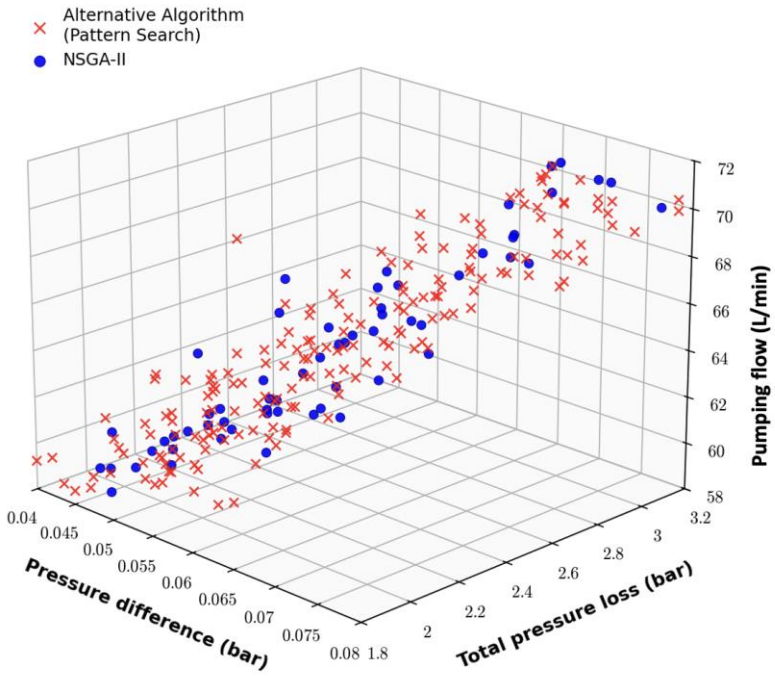


Figure 9. Comparison of Pareto fronts: NSGA-II vs. Alternative algorithm

3.6 Comparison Before and After Optimization

The flow value from the optimized design combination with a flow weight of 0.2 was substituted into the pre-optimization AMESim model for calculation, and the corresponding values obtained were compared with the optimized solution combination, as shown in Table 7. By comparing the values before and after optimization, it can be concluded that after optimization, the casing pressures of the two motors on Side A and Side B of the flushing circuit were reduced from 0.7954 to 0.7779 bar and from 0.7311 to 0.7201 bar, which were reduced by 2.2% and 1.5% compared with those before optimization, respectively; the pressure differential between the two motor casings was reduced from 0.0643 to 0.0578 bar, which was reduced by 10.1% compared with the unoptimized state; and the total pressure loss was reduced from 2.2943 to 2.276 bar, which was reduced by 0.8% compared with the unoptimized state. Although the 0.8% reduction in the total pressure loss appears marginal in terms of energy savings, the primary engineering significance of this

optimization lies in equipment safety. Notably, the casing pressure differential was reduced by 10.1% (from 0.0643 to 0.0578 bar). Given that the shaft seals of such large-scale motors are highly vulnerable to asymmetric pressure loads (with a tolerance typically below 3 bar), this 10.1% improvement is significant. This effectively minimizes eccentric wear on the seals during weeks of continuous testing. Therefore, the enhanced operational reliability far outweighs the computational costs introduced by the optimization framework. To quantitatively contextualize these optimization margins, recent benchmark studies on simpler or isolated hydraulic networks [27] reported single-objective pressure loss reductions of approximately 9.0%. Although the 0.8% pressure loss reduction achieved in this study appears numerically smaller than such benchmarks, it represents a strictly constrained optimum within a strongly coupled multi-objective framework. In this parallel flushing circuit, attempting to force a 9% reduction in the pressure loss would necessitate an unacceptable drop in the cooling flow rate or trigger a severe spike in the casing pressure differential, immediately leading to thermal or mechanical failure. Therefore, securing a dominant 10.1% improvement in the critical mechanical safety metric (pressure differential) while simultaneously maintaining a net-positive reduction in the total pressure loss demonstrates the superior practical effectiveness of this framework compared to traditional single-objective benchmarks.

Beyond numerical improvements, this study offers significant theoretical and practical advancements. Theoretically, we proposed a 'continuous search, discrete decoding' strategy that resolves the inherent conflict between algorithmic continuity and the discrete nature of industrial components, providing a robust mathematical template for optimization in complex parallel hydraulic architectures. Practically, the established surrogate-assisted framework offers a validated and computationally efficient roadmap for designing and maintaining large-scale motor test benches. By quantitatively revealing the physical trade-off boundaries between heat dissipation and mechanical safety, this study enables engineers to systematically enhance equipment reliability and adapt to diverse testing loads through flexible decision-making, transcending the limitations of traditional empirical design methods.

Table 7. Parameter comparison before and after optimization

	Parameter	Pre-optimization	Post-optimization	Reduction rate
Parameters values	Pipeline A length/m	9.3	9.5	
	Pipeline B length/m	10.5	9.04	
	A Number of elbows	8	5	
	B Number of elbows	8	7	
Objective values	Case A pressure/bar	0.7954	0.7779	2.2%
	Case B pressure/bar	0.7311	0.7201	1.5%
	Pressure differential/bar	0.0643	0.0578	10.1%
	Total pressure loss/bar	2.2943	2.2760	0.8%

4. Conclusions

To address the strong physical conflicts among the flushing flow, casing pressure, and pipeline pressure loss in parallel hydraulic circuits, this study established a surrogate-assisted multi-objective optimization framework. By integrating Maximin Latin Hypercube Sampling (MLHS), high-precision Kriging models, and the NSGA-II algorithm, the complex nonlinear interactions within the large-scale motor test bench were effectively decoupled. The systematic integration of these methods enables a comprehensive exploration of the design space while maintaining high computational efficiency. The optimization results directly resolve the initial engineering contradictions. Under balanced TOPSIS decision-making, the casing pressure differential, the most critical metric for motor seal safety, was reduced by 10.1%, while the total circuit pressure loss was simultaneously decreased by 0.8% without compromising the required flushing flow rate. These quantitative improvements demonstrate that the proposed framework effectively reconciles the conflicting demands of heat dissipation, energy efficiency, and mechanical reliability of the material. This study provides a robust technical roadmap and validated decision-making tool for the multi-objective optimization of complex parallel hydraulic systems.

Finally, this study has several limitations. First, the current optimization is based on static simulation models and does not consider transient thermal-fluid fluctuations or pipe vibrations during rapid pressure shifts. Second, although the MLHS-Kriging framework is robust, the training dataset is specific to the Hägglunds CB400 motor test bench; thus, generalizing the results to significantly different hydraulic architectures would require supplementary sampling. Future research will focus on integrating dynamic fluid-structure interactions and developing a more universal surrogate model for diverse parallel hydraulic systems.

Acknowledgements

The authors sincerely thank Prof. Bing Zhang for his continuous guidance and valuable suggestions throughout this study. All individuals named in this section have consented to be acknowledged in this study.

Funding

This study did not receive any funding from public, private, or not-for-profit funding bodies.

Declaration of Competing Interests

The authors declare no conflict of interest.

CRediT Author Contribution Statement
Yan Cao: Conceptualization; Methodology; Software; Data curation; Writing - original draft; Visualization
Bing Zhang: Validation; Investigation; Resources; Data curation; Writing - review & revise
Jingding Tian: Software; Analysis; Validation; Writing - review & revise
Jiawei Wu: Software; Analysis; Writing - review & revise
Hongyu Lu: Investigation; Writing - review & revise
Hao Chen: Conceptualization; Writing - review & revise; Supervision; Project administration

Availability of Data and Materials
The data supporting the findings of this study are available from the corresponding author upon request.

Ethics Statement
This study did not involve human participants or animal subjects. Therefore, ethical approval was not required.

Generative Artificial Intelligence Disclosure
The authors claim that artificial intelligence-assisted technologies, such as generative AI, were not used to generate content, ideas, or theories. We have used AI to enhance readability and refine the language. This was used with extreme human control and supervision. The authors take full responsibility for reviewing and approving the content of this manuscript.

References

[1] H. Mu, Y. Luo, Y. Luo, *et al.*, "Numerical analysis of energy recovery of hybrid loader actuators based on parameters optimization," *Actuators*, vol. 11, no. 9, Art. no. 260, 2022. https://doi.org/10.3390/act11090260.

[2] H. Zhang, W. Wei, H. Wang, *et al.*, "Digital hydraulic motor characteristic analysis for heavy-duty vehicle traction," *Actuators*, vol. 14, no. 1, Art. no. 11, 2025. https://doi.org/10.3390/act14010011.

[3] H. Zhao, H. Xie, Y. Zhao, *et al.*, "Coordinated electro-hydraulic composite braking method for improving energy recovery in emergency braking," *IEEE Transactions on Transportation Electrification*, vol. 11, no. 5, pp. 11017–11029, 2025. https://doi.org/10.1109/TTE.2025.3569924.

[4] P. S. Mahankar and A. S. Dhoble, "Review of hydraulic seal failures due to effect of medium to high temperature," *Engineering Failure Analysis*, vol. 127, Art. no. 105552, 2021. https://doi.org/10.1016/j.engfailanal.2021.105552.

[5] P. S. Mahankar, A. S. Dhoble, and R. Prabhu, "Experimental investigation of polyurethane seal failure used in hydraulic system," *Engineering Failure Analysis*, vol. 150, Art. no. 107319, 2023. https://doi.org/10.1016/j.engfailanal.2023.107319.

[6] S. Liu, A. Ben-Abdelwahed, A. Sommier, *et al.*, "Experimental investigation of leakage flow measurement and surface morphology in small-scale liquid mechanical seals," *Flow Measurement and Instrumentation*, vol. 106, Art. no. 102957, 2025. https://doi.org/10.1016/j.flowmeasinst.2025.102957.

[7] D. Li, X. Liu, R. Nie, *et al.*, "Simulation analysis on flow field of aircraft hydraulics bent pipe with guide vane," in *2023 Asia-Pacific International Symposium on Aerospace Technology (APISAT 2023) Proceedings*, *Lecture Notes in Electrical Engineering*. 2024, pp. 535–545. https://doi.org/10.1007/978-981-97-4010-9_39.

[8] M. Wang, D. Li, X. Liu, *et al.*, "Comparative analysis of guide vane edge profiles in LPBF-manufactured elbows for enhanced flow performance," *Ocean Engineering*, vol. 357, Art. no. 125280, 2026. https://doi.org/10.1016/j.oceaneng.2026.125280.

[9] D. Li, N. Dai, H. Wang, and F. Zhang, "Mathematical modelling study of pressure loss in the flow channels of additive manufacturing aviation hydraulic valves," *Energies*, vol. 16, no. 4, Art. no. 1788, 2023. https://doi.org/10.3390/en16041788.

[10] C. K. Park, K. P. Jang, J. H. Jeong, Y. S. Sohn, and S. H. Kwon, "Analysis on Pressure Losses in Pipe Bends Based on Real-Scale Concrete Pumping Tests," *ACI Materials Journal*, vol. 117, no. 3, pp. 205–216, 2020. https://doi.org/10.14359/51724616.

[11] A. Ebrahimi-Moghadam, S. Kowsari, F. Farhadi, *et al.*, "Thermohydraulic sensitivity analysis and multi-objective optimization of Fe3O4/H2O nanofluid flow inside U-bend heat exchangers with longitudinal strip inserts," *Applied Thermal Engineering*, vol. 164, Art. no. 114518, 2020. https://doi.org/10.1016/j.applthermaleng.2019.114518.

[12] R. Zhang, X. Guo, Y. Liu, *et al.*, "Pressure loss in the vertical hydraulic transport of seabed mineral particles," *Powder Technology*, vol. 469, Art. no. 121763, 2026. https://doi.org/10.1016/j.powtec.2025.121763.

[13] I. Bogrekci, P. Demircioglu, O. Kozaka, *et al.*, "Revealing and minimizing hidden energy losses in hydraulic lines of mobile machinery," *Thermal Science*, vol. 29, no. 4 Part B, pp. 3061–3074, 2025. https://doi.org/10.2298/TSCI2504061B.

[14] J. Gao, Y. Shi, Y. Xu, *et al.*, "Principle and pressure loss experiment of electro-hydraulic slide-rotary direction valve in single-pump and multi-motor hydraulic system," *Advances in Mechanical Engineering*, vol. 16, no. 10, 2024. https://doi.org/10.1177/16878132241284346.

[15] S. Thakur, A. Kumar, and S. Singh, "A critical review of the various energy-saving models used in hydrostatic power transmission drives for enhancing the efficiency of chairlift transport system," *Arabian Journal for Science and Engineering*, vol. 49, no. 8, pp. 10327–10348, 2024. https://doi.org/10.1007/s13369-023-08608-9.

[16] S. Liu, W. Xie, Q. Wang, *et al.*, "Thermal performance of a central-jetting microchannel heat sink designed for a high-power laser crystal," *International Journal of Heat and Mass Transfer*, vol. 185, Art. no. 122409, 2022. https://doi.org/10.1016/j.ijheatmasstransfer.2021.122409.

[17] J.-S. Park, L. D. Tai, and M.-Y. Lee, "numerical study on the heat transfer characteristics of a hybrid direct–indirect oil cooling system for electric motors," *Symmetry*, vol. 17, no. 5, Art. no. 760, 2025. https://doi.org/10.3390/sym17050760.

[18] X. Luo, Z.-N. Yang, J. Zhang, *et al.*, "Effect of guide vane on pressure loss and heat transfer characteristics of supercritical CO_2 in U-shaped channel," *Journal of Thermal Science*, vol. 31, no. 3, pp. 701–711, 2022. https://doi.org/10.1007/s11630-022-1530-z.

[19] Z. Yan, G. Tang, and Y. Gao, "Research on pressure control of hydraulic system for pump controlled anchor drilling machine based on variable universe fuzzy PID algorithm," *Machines*, vol. 13, no. 3, Art. no. 199, 2025. https://doi.org/10.3390/machines13030199.

[20] A. Bonavolontà, E. Frosina, P. Marani, D. Mesturini, C. Dolcin, and U. Busani, "Experimental and modelling analysis of a downstream compensation system: energy optimization of the directional control valves," *International Journal of Fluid Power*, vol. 24, no. 1, pp. 99-124, 2023. https://doi.org/10.13052/ijfp1439-9776.2415.

[21] H. Wu, Y. Dong, G. Cao, *et al.*, "Logic design method and optimization of hydraulic system for heavy-duty automatic transmission," *Transactions of the Canadian Society for Mechanical Engineering*, vol. 47, no. 1, pp. 143–153, 2023. https://doi.org/10.1139/tcsme-2021-0042.

[22] W. Ullah, M. A. N. Mu'tasim, and M. F. F. Rashid, "Optimization of cost-based hybrid flowshop scheduling using teaching-learning-based optimization algorithm," *International Journal of Automotive and Mechanical Engineering*, vol. 21, no. 3, pp. 11616–11628, 2024. https://doi.org/10.15282/ijame.21.3.2024.13.0896.

[23] L. Han, L. Yang, and L. Su, "Energy storage configuration and scheduling for rail transit based on a beetle antennae-optimized back propagation neural network prediction algorithm," *International Journal of Automotive and Mechanical Engineering*, vol. 22, no. 4, pp. 12970–12985, 2025. https://doi.org/10.15282/ijame.22.4.2025.10.0987.

[24] W. Lu, "Optimization design of electromechanical servo system based on dual motor control algorithm," *International Journal of Automotive and Mechanical Engineering*, vol. 22, no. 1, pp. 12162–12173, 2025. https://doi.org/10.15282/ijame.22.1.2025.16.0933.

[25] K. Deb, A. Pratap, S. Agarwal, and T. Meyarivan, "A fast and elitist multi-objective genetic algorithm: NSGA-II," *IEEE Transactions on Evolutionary Computation*, vol. 6, no. 2, pp. 182–197, 2002. https://doi.org/10.1109/4235.996017.

[26] Suprayitno and M. Y. Pratama, "Multi-objective optimization of three-pass perforated muffler design for improved acoustic performance and reduced fluid pressure drop using genetic algorithms," *International Journal of Automotive and Mechanical Engineering*, vol. 22, no. 1, pp. 12074–12090, 2025. https://doi.org/10.15282/ijame.22.1.2025.10.0927.

[27] Z. Zheng, N. Chen, X. Yuan, *et al.*, "Analysis and optimization of multi-physical field coupling in boom flow channel of excavator multi-way valves," *Machines*, vol. 12, no. 9, Art. no. 611, 2024. https://doi.org/10.3390/machines12090611.

[28] Y. Yue, Y. Li, and X. Zuo, "Optimization of subsea production control system layout considering hydraulic fluid pressure loss," *Ocean Engineering*, vol. 288, Art. no. 116047, 2023. https://doi.org/10.1016/j.oceaneng.2023.116047.

[29] J. Wang, C. Hu, D. Du, *et al.*, "Multi-objective optimization of multiphase pump by using computational fluid dynamics and non-dominated sorting genetic algorithm II," *Renewable Energy*, vol. 254, Art. no. 123717, 2025. https://doi.org/10.1016/j.renene.2025.123717.

[30] K. Mohammadi and S. Bagheri, "Prefabricated broad-crested weirs: a novel sustainability framework integrating hydraulic optimization, cost, and embodied carbon," *Water Conservation Science and Engineering*, vol. 11, no. 1, Art. no. 19, 2026. https://doi.org/10.1007/s41101-026-00491-3.

[31] L. Zeng, D. Zhang, Y. Li, and J. Jiang, "A novel multi-objective optimization method based on enhanced hippopotamus optimization algorithm and Kriging model," *International Journal of Structural Integrity*, vol. 16, no. 6, pp. 1331–1354, 2025. https://doi.org/10.1108/IJSI-04-2025-0105.

[32] M. E. Johnson, L. M. Moore, and D. Ylvisaker, "Minimax and maximin distance designs," *Journal of Statistical Planning and Inference*, vol. 26, no. 2, pp. 131–148, 1990. https://doi.org/10.1016/0378-3758(90)90122-B.